Characterization of the breakup channel in the asymmetric systems ^{40,48}Ca $+$ ^{12}C at 25 and 40 MeV/nucleon

S. Piantelli [1,*] G. Casini,[1] P. Ottanelli,[1] L. Baldesi,[2,1] S. Barlini,[2,1] B. Borderie,[3] R. Bougault,[4] A. Camaiani,[5,†] A. Chbihi,[6] C. Ciampi,[2,1,‡] J. A. Dueñas,[7] D. Fabris,[8] Q. Fable,[9] J. D. Frankland,[6] C. Frosin,[2,1] F. Gramegna,[10] D. Gruyer,[4] B. Hong,[11,12] A. Kordyasz,[13] T. Kozik,[14] M. J. Kweon,[15] J. Lemarié,[6] N. LeNeindre,[4] I. Lombardo,[16,17] O. Lopez,[4] T. Marchi,[10] K. Mazurek,[18] S. H. Nam,[11,12] M. Pârlog,[4,19] J. Park,[11,12] G. Pasquali,[2,1] G. Poggi,[2,1] A. Rebillard-Soulié,[4] A. A. Stefanini,[2,1] S. Upadhyaya,[14] S. Valdré,[1] G. Verde,[16,9] E. Vient,[4] and M. Vigilante[20,21]

(FAZIA Collaboration)

[1]*INFN Sezione di Firenze, I-50019 Sesto Fiorentino, Italy*
[2]*Dipartimento di Fisica, Università di Firenze, I-50019 Sesto Fiorentino, Italy*
[3]*Université Paris-Saclay, CNRS/IN2P3, IJCLab, F-91405 Orsay, France*
[4]*Normandie Université, ENSICAEN, UNICAEN, CNRS/IN2P3, LPC Caen, F-14000 Caen, France*
[5]*Instituut voor Kern-en Stralingsfysica, KU Leuven, B-3001 Heverlee, Belgium*
[6]*GANIL, CEA/DRF-CNRS/IN2P3, F-14076 Caen, France*
[7]*Departamento de Ingenierá Eléctrica y Centro de Estudios Avanzados en Física, Matemáticas y Computación,
Universidad de Huelva, 21007 Huelva, Spain*
[8]*INFN Sezione di Padova, I-35131 Padova, Italy*
[9]*Laboratoire des 2 Infinis - Toulouse (L2IT-IN2P3), Université de Toulouse, CNRS, UPS, F-31062 Toulouse Cedex 9, France*
[10]*INFN Laboratori Nazionali di Legnaro, I-35020 Legnaro, Italy*
[11]*Center for Extreme Nuclear Matters (CENuM), Korea University, Seoul 02841, Republic of Korea*
[12]*Department of Physics, Korea University, Seoul 02841, Republic of Korea*
[13]*Heavy Ion Laboratory, University of Warsaw, PL-02093 Warszawa, Poland*
[14]*Faculty of Physics, Astronomy and Applied Computer Science, Jagiellonian University, PL-30348 Kraków, Poland*
[15]*Department of Physics, Inha University, Incheon 22212, Republic of Korea*
[16]*INFN Sezione di Catania, I-95123 Catania, Italy*
[17]*Dipartimento di Fisica e Astronomia, Università di Catania, I-95123 Catania, Italy*
[18]*Institute of Nuclear Physics Polish Academy of Sciences, PL-31342 Kraków, Poland*
[19]*"Horia Hulubei" National Institute of Physics and Nuclear Engineering (IFIN-HH), RO-077125 Bucharest Magurele, Romania*
[20]*Dipartimento di Fisica, Università di Napoli, I-80126 Napoli, Italy*
[21]*INFN Sezione di Napoli, I-80126 Napoli, Italy*

An analysis of the asymmetric reactions ^{40,48}Ca $+$ ^{12}C at 25 and 40 MeV/nucleon is presented. Data were collected with six modules of the FAZIA array. The analysis is focused on the breakup channel of sources produced in dissipative collisions, partially corresponding to incomplete fusion processes. The study was performed both on detected fragments and on some resonances reconstructed by means of particle-fragment correlations, with a focus on the evolution of the breakup channel with the beam energy and the neutron content of the system, looking in particular at the relative velocity between the breakup fragments. Results show that also carbon fragments reconstructed by means of particle correlations can be in large part interpreted as the light partner of a scission.

I. INTRODUCTION

The investigation of the breakup channel in heavy ion collisions at Fermi energies is a topic widely represented in the literature for many years. In particular, efforts have been made to study the emission pattern of the fragments coming from the quasiprojectile (QP) breakup [1–10]. For example, one goal is the investigation of the differences between this process and a pure low-energy fission modeled in terms of the nuclear structure and statistical arguments. In particular, a correlation between the scission timescales, the breakup configuration, and the split asymmetry has been found: for large mass asymmetry, the lighter partner is preferentially emitted in the backward direction and on fast times,

---

*Corresponding author: silvia.piantelli@fi.infn.it

†Present address: Dipartimento di Fisica, Università di Firenze, I-50019 Sesto Fiorentino, Italy.

‡Present address: GANIL, CEA/DRF-CNRS/IN2P3, F-14076 Caen, France.

therefore this process was called fast oriented fission [1,3,11,12]. More recently, very refined investigations were carried out [6,7] also by our collaboration [9,10] concerning the isotopic composition of both QP breakup fragments in coincidence. In particular, in [6,7] the isotopic composition of the breakup partners (with more sensitivity for the lighter one) was found to be correlated with the breakup configuration: when the light fragment is backward emitted towards the center of mass (c.m.) of the system, i.e., in configurations typical of the fast oriented fission, it is more neutron rich than when emitted in the opposite direction. According to the general consensus on this subject [3,5], also recently reinforced by theoretical analyses [13], the authors of the papers [6,7] interpreted the angle between the QP breakup axis and the QP-QT (quasitarget) separation axis (often labeled as α or θ_{PROX}) as a clock of the fission process, and they extracted a timescale of about 100 fm/c for the equilibration of the isospin degree of freedom within the QP. In [10], in the limit of the available statistics, a similar analysis was performed, finding a correlation of the isospin versus angle α in substantial agreement with the results of [6,7]. The experimental data were also found to be quite consistent with the predictions of the antisymmetrized molecular dynamics model (AMD) [14–18]. However, the interpretation of the α angle as a clock of the fission process (and of the isospin equilibration) was not obvious within the framework of AMD.

The above discussion on the breakup pertains to rather symmetric collisions between relatively heavy nuclei that are dominated by a large yield of almost binary events with two main QP and QT ejectiles; as discussed above, these deformed and excited nuclei can then undergo a breakup process with different mass asymmetries possibly associated with various timescales. Obviously, at Fermi beam energies (i.e., in the range 20–50 MeV/nucleon) a fissionlike process can occur not only for QP and/or QT in semiperipheral collisions but also for composite sources produced in incomplete fusion events. Fusionlike events are a minority in the case of heavy systems but they can generally be favored moving to lighter and more asymmetric reactions [19]. For mass asymmetric systems, the contribution of binary dissipative collisions is confined at rather peripheral reactions. At energies just above the Coulomb barrier, reactions of the fusion type dominate at almost all the impact parameters, with the formation of a unique major excited source. With increasing beam energy, fast emissions of nucleons or clusters during the interaction (before the formation of a "true" compound nucleus) become more important, thus favoring the incomplete fusion channel. The rest of the reaction cross section for asymmetric medium-light systems and at Fermi energies corresponds to a broad distribution of more or less damped collisions with the formation of excited sources which further break up and decay. Of course, the distinction between very dissipative binary reactions and incomplete fusion is faint; in particular for asymmetric systems, also taking into account the broadening due to fast emissions, it is difficult to disentangle the sources produced through incomplete fusions or through damped (binary) reactions by using the measured products. Indeed, from the experimental point of view, the overlap of concurrent processes generates a broad spectrum of primary

sources which then decay towards stable states; in reverse kinematics measurements, which are often done, this corresponds to the observation at forward angles of a wide range of fragments with sizes not too far from that of the projectile and velocities extending from those of the beam to that of the c.m. The experimental data discussed in this paper refer to reactions of this kind.

To our knowledge, medium-light asymmetric systems have not been widely studied, in recent years, with regard to the characterization of the breakup channel. Indeed, the reactions discussed in this paper, using Ca beams of different isotopes provide also information about the role of the neutron richness of the system in the source breakup. In fact, this work deals with the analysis of experimental data collected with six FAZIA blocks for the systems ^{48,40}Ca + ^{12}C at 25 MeV/nucleon and ^{48}Ca + ^{12}C at 40 MeV/nucleon (referred to as the FAZIAPRE experiment). The main focus of the paper is on the breakup channel, for which we were able to attempt detailed analysis also benefiting the isotopic identification of both breakup partners. In particular we investigated their relative velocity as a function of the charge asymmetry of the splitting and of the reconstructed source size. Moreover, the particle correlation technique was applied to reconstruct some resonances of carbon isotopes, showing that also these excited fragments can be interpreted as light ejectiles of a breakup process.

II. THE EXPERIMENT

Pulsed beams of ^{48,40}Ca at 25 and 40 MeV/nucleon, with average current of 0.1 p nA, were delivered by the CS cyclotron of INFN-LNS in Catania and impinged on a ^{12}C target with a thickness of about 300 μg cm^{-2}. The system ^{40}Ca at 40 MeV/nucleon presents some calibration issues and it is not included in the following analysis. Data were collected with six FAZIA blocks, four of them placed in a wall configuration (1 m from the target) and covering the polar angles between 1.7° and 7.6° in the laboratory frame, and two of them located on the equatorial plane on opposite sides (polar angle range 11.5°–16.7°). The layout of the experimental setup in polar representation is shown in Fig. 1 while in Table I some properties of the investigated reactions are summarized.

The whole setup was housed inside the Ciclope scattering chamber of INFN-LNS. The FAZIA blocks have been described in detail elsewhere (see for example [20–24] and references therein). Here we briefly recall that each block includes 16 three-stage telescopes [300-μm-thick silicon, 500-μm-thick silicon, 10-cm-thick CsI(Tl)]. The preamplifiers and the fast digitizing electronic boards operate under vacuum with proper cooling. State-of-the-art capabilities in terms of isotopic identification have been achieved for these detectors [22,24].

Because of the strongly reversed kinematics of the investigated reactions, the detection efficiency of the setup is favored at least for medium-heavy ejectiles. In fact, the efficiency for big fragments ($Z \geqslant 10$) is around 34%, 41%, and 19% for ^{40}Ca at 25 MeV/nucleon, ^{48}Ca at 25 MeV/nucleon, and ^{48}Ca at 40 MeV/nucleon, respectively; these values were estimated by means of a simulation based on the HIPSE code [25],
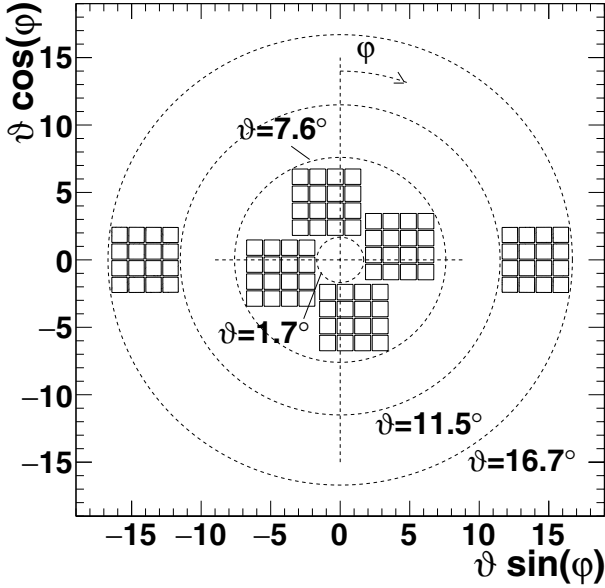
FIG. 1. Layout of the experimental setup in polar representation.

filtered via a software replica of the setup which takes into account the geometry and the identification thresholds. The global efficiency for all the reaction channels is significant (around 41% for ^{40}Ca at 25 MeV/nucleon, around 46% for ^{48}Ca at 25 MeV/nucleon and around 30% for ^{48}Ca at 40 MeV/nucleon). In contrast, the efficiency for light particles is limited (around 2% for $Z = 1$ and around 4–5% for $Z = 2$ for all systems) as expected, due to their much broader angular distribution. The global efficiency was calculated as the fraction of simulated events surviving the experimental filter with at least one detected ejectile independently of the reaction mechanism, while that for big fragments (light particles) was obtained as the fraction of simulated fragments with $Z \geqslant 10$ (particles with $Z = 1, 2$) surviving the experimental filter. As a consequence, although the detection of complete events (in charge) is hindered and we cannot attempt selections and analyses based on the event completeness, medium-heavy ejectiles can still be reliably characterized.

III. DATA ANALYSIS

A. A general overview of the reactions

The studied systems are strongly mass asymmetric and thus—as shown in Table I—the c.m. velocity is close to the

projectile velocity. On the one hand this helps focusing most of the ejecta in a narrow forward cone, thus enlarging the acceptance in the c.m. frame, as quantified above. On the other hand the velocities of the heaviest fragments, from peripheral collisions to more central ones, span a narrow interval.

This is illustrated in Fig. 2, where, in panel (a), the experimental charge–laboratory velocity correlation for all reaction products is shown for the ^{48}Ca at 25 MeV/nucleon beam; the corresponding velocity and charge distributions are shown in panels (c) and (d) [in panel (d) the charge distribution is presented for $Z > 2$]. A spot located between c.m. (dotted arrow) and beam velocity (continuous arrow), with $Z \gtrsim 15$ and peaked around $Z = 20$ [apparent in panel (d)] and with velocity almost independent of the charge, is clearly evident; this region mainly corresponds to more or less damped events. The quasielastic reactions producing weakly excited QT and QP nuclei are not evident in these data, because their detection is significantly reduced by the angular coverage of the setup. In fact the grazing angles (see Table I) are well below the minimum angle covered by the array for all the reactions. For lower charges ($Z < 14$) two branches emerge, one at $v_{\mathrm{lab}} > v_{\mathrm{c.m.}}$ and one at $v_{\mathrm{lab}} < v_{\mathrm{c.m.}}$, compatible with the breakup (henceforth BU) of the heavier nuclei around calcium produced by strongly damped collisions. This is better put into evidence in the inset of Fig. 2(a), where we show the charge–laboratory velocity correlation for the biggest and the second biggest fragments of the event, both of them with $Z \geqslant 5$, according to the BU selection introduced in Sec. III B. The corresponding laboratory velocity and charge distributions are presented in the insets of panels (c) and (d). Two asymmetric branches, with the one at velocities greater than $v_{\mathrm{c.m.}}$ being more populated, are apparent in the inset of panel (c). In the charge distribution [inset of panel (d)] two regions emerge, basically corresponding to the light (below $Z = 10$) and the heavy (beyond $Z = 10$) BU fragment, as will be better shown in Fig. 4. The efficiency for BU events, estimated as the fraction of simulated events with at least two fragments with $Z \geqslant 5$ surviving the experimental filter, is below 1% for all the reactions. The efficiency for the events in which a $Z \geqslant 5$ fragment is accompanied only by light ejectiles with $Z < 5$ is around 8–10% for all reactions and it decreases by about 1% when requiring that the charge of the heavy residue is $Z \geqslant 10$ and that it is isotopically identified.

In order to shed more light on the reaction mechanism, the experimental data were compared with a simulation based on the the AMD code [14,15,18] coupled to GEMINI++ [26] as an afterburner, as already successfully done to study

TABLE I. Some characteristics of the investigated reactions. $(N/Z)_{\mathrm{proj}}$ and $(N/Z)_{\mathrm{sys}}$ are the isotopic compositions of the projectile and of the whole system, respectively. $\vartheta_{\mathrm{graz}}$ and b_{graz} are the grazing angle in laboratory and the grazing impact parameter, respectively. $v_{\mathrm{c.m.}}$, v_{beam}, and $v_{\mathrm{beam}}^{\mathrm{c.m.}}$ are the c.m. velocity and the beam velocities in laboratory and in c.m., respectively.

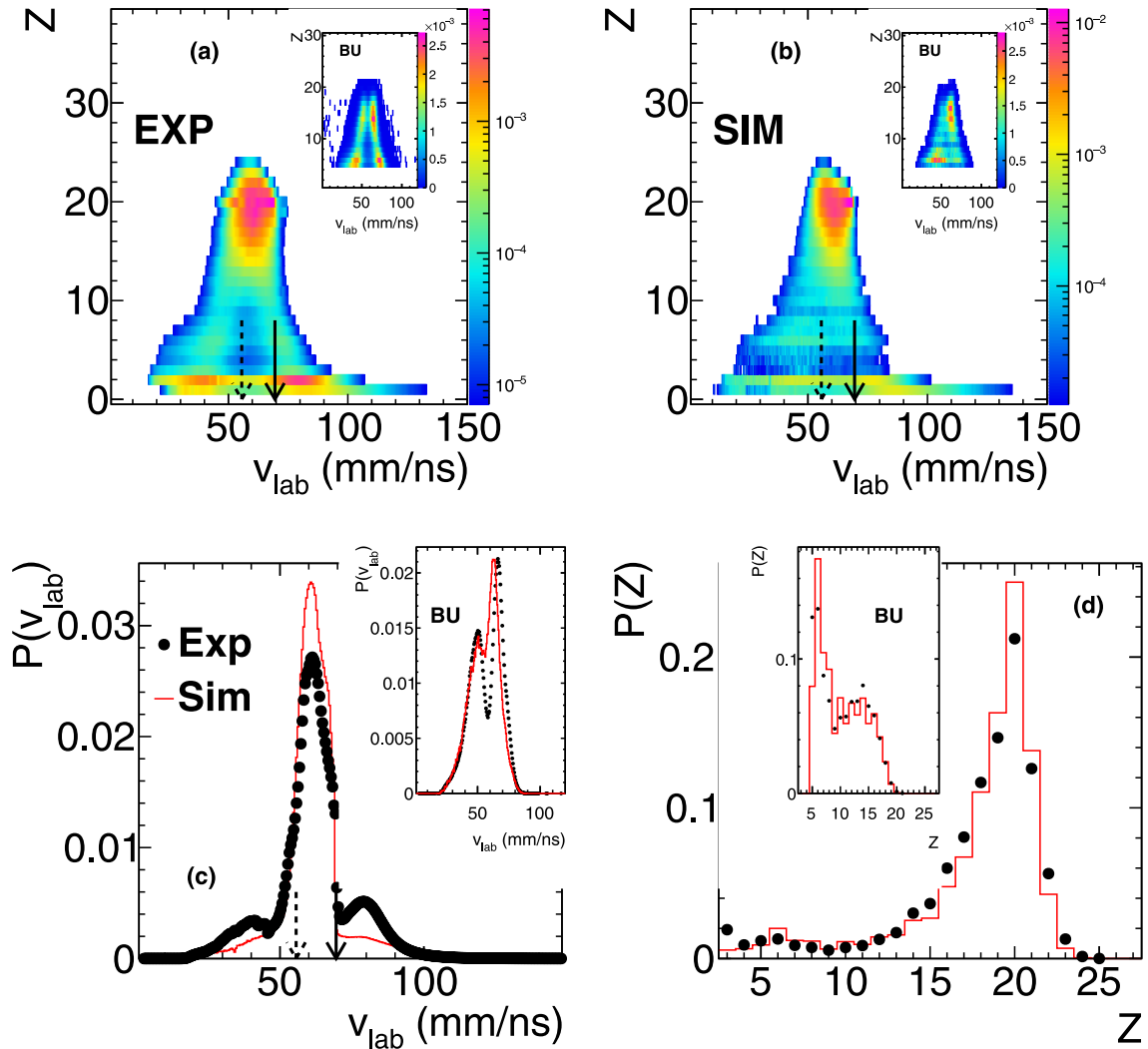| Beam MeV/nucleon	$(N/Z)_{\mathrm{proj}}$	$(N/Z)_{\mathrm{sys}}$	$\vartheta_{\mathrm{graz}}$ (deg)	b_{graz} (fm)	$v_{\mathrm{c.m.}}$ (mm/ns)	v_{beam} (mm/ns)	$v_{\mathrm{beam}}^{\mathrm{c.m.}}$ (mm/ns)
^{40}Ca@25	1.0	1.0	1.0	8.6	53.5	69.5	16.0
^{48}Ca@25	1.4	1.31	0.9	8.8	55.6	69.5	13.9
^{48}Ca@40	1.4	1.31	0.5	8.9	70.3	87.9	17.6

FIG. 2. ^{48}Ca + ^{12}C at 25 MeV/nucleon. (a) Charge–laboratory velocity correlation for all the ejectiles, experimental data; in the inset the correlation for the biggest and the second biggest fragment of the event for the BU selection is shown. (b) The same as in panel (a) but for AMD+GEMINI++ simulation filtered via a software replica of the setup. (c) Relative probability distribution of laboratory velocity for all the ejectiles; symbols (red [light gray] histogram without symbols): experimental (simulated) data. The dotted (continuous) arrow corresponds to the c.m. (beam) velocity. In the inset the projection on the velocity axis of the insets of panels (a) and (b) is shown. (d) Relative probability distribution of charge for $Z > 2$; symbols (red [light gray] histogram without symbols): experimental (simulated) data. In the inset the projection on the charge axis of the insets of panels (a) and (b) is shown.

other FAZIA experiments [9,10,27–29]. Details concerning the used version of the code can be found in [10,30]. The simulated data, filtered through a software replica of the setup, are shown in Figs. 2(b) and 2(c) [red (light gray) histogram without symbols] and (d) [red (light gray) histogram without symbols] and reasonably reproduce the experimental ones. In fact the same spot at high Z as in the experimental case is present and the overall charge distribution is well reproduced [as shown in panel (d) for $Z > 2$]. However, the two velocity branches, especially in the low-Z region from lithium to boron, are less separated, as is apparent in the inset of panel (c) when the BU selection is applied. In particular, the branch at velocity greater than $v_{c.m.}$ is shifted towards lower values with respect to the experimental case. On the other side, the charge

distribution is reasonably reproduced also for BU events [inset of panel (d)].

Concerning light products, channels involving α particles are expected to be abundant in reactions with a ^{12}C target in particular for the $N = Z$ projectile case [31,32]. In fact, as shown in Fig. 3, events with at least three α represent about 0.1% of the total, thus they are sufficient to study α particle correlations, such as those coming from the deexcitation of ^{12}C*. The picture shows that, although the detection efficiencies for α particles are very similar for all the reactions, in the case of ^{48}Ca beams events with many α are more abundant for the reaction at 40 MeV/nucleon than for that at 25 MeV/nucleon, due to the higher available energy favoring in general nuclear fragmentation. The ^{40}Ca beam, although at 25
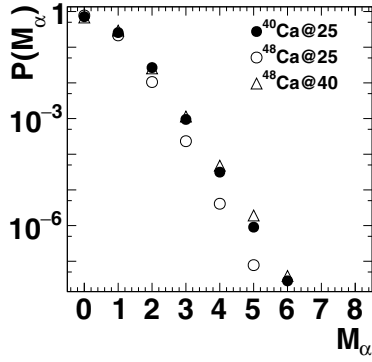
FIG. 3. Relative probability distribution of α particle multiplicity for all the measured reactions.

MeV/nucleon, shows α multiplicities close to the ^{48}Ca at 40 MeV/nucleon case, probably due to the nature of the system where both target and projectile are α conjugate.

B. Breakup (BU) channel

Keeping in mind that the collected events are mainly related to strongly damped collisions with the formation of a heavy excited source, the BU channel is selected by requiring events with two fragments with $Z \geqslant 5$ each, labeled as HF (heavy fragment, with charge Z_{HF} and mass A_{HF}) and LF (light fragment, with charge Z_{LF} and mass A_{LF}). The associated reconstructed parent nucleus (henceforth denoted as BU fragment or BUF, with charge $Z_{BU} = Z_{HF} + Z_{LF}$ and mass $A_{BU} = A_{HF} + A_{LF}$) has therefore $Z \geqslant 10$, a value roughly corresponding to the lower limit of the peak of the charge distribution of the biggest detected fragments [see Fig. 2(d)].

Before discussing in detail the properties of the BU channel, we mention that in the experimental sample the fraction of BU events with respect to the number of events (from now on labeled as "residue" or R events) with one fragment with $Z \geqslant 10$ (henceforth called residue or R fragment, with charge Z_R and mass A_R) and at least another ejectile with $Z < 5$ is 14–15% for all reactions.

1. Source size and asymmetry of the split

For all systems the BU favors asymmetric splits as expected for the binary division of light nuclei (fissionlike channel, where surface and Coulomb energies dominate the process), quite below the Businaro-Gallone region. An example of this is shown in Fig. 4(a), which presents the Z_{LF} vs Z_{HF} plot for the ^{48}Ca + ^{12}C reaction at the lower energy; defining η as the charge asymmetry (i.e., $\eta = \frac{Z_{HF} - Z_{LF}}{Z_{HF} + Z_{LF}}$), the BU yield concentrates at $\eta > 0.3$. More quantitatively Fig. 4(b) compares the experimental asymmetries for the BU measured in the three reactions. The most asymmetric BU occurs for the neutron rich system at the lower energy while at 40 MeV/nucleon the ^{48}Ca reaction produces an asymmetry comparable with that of ^{40}Ca beam collisions at low energy. Figures 4(c) and 4(d) separately show the Z_{HF} and Z_{LF} distributions, for the three systems. A hierarchy can be seen: mainly for HF, but also to a lesser extent for LF, the distributions
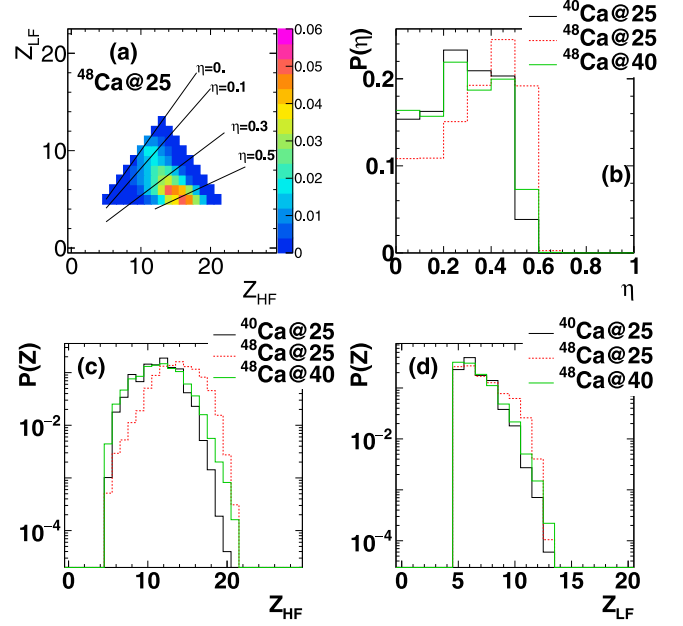

FIG. 4. (a) Z_{LF} vs Z_{HF} correlation for ^{48}Ca at 25 MeV/nucleon. For all systems, relative probability distribution of (b) η, (c) Z_{HF}, (d) Z_{LF}.

obtained for the ^{48}Ca beam at 25 MeV/nucleon are shifted towards higher values with respect to the other cases. The ^{48}Ca beam at 40 MeV/nucleon gives values slightly heavier than the ^{40}Ca case. These effects are possibly due to the fact that the ^{48}Ca beam, being more neutron rich, can keep bound larger fragments with respect to the ^{40}Ca case, but when the energy increases longer decay chains are expected due to the higher excitation energy deposited in the system; also the dynamical emissions of particles (most likely, but not exclusively, neutrons for the n-rich projectile), again increasing with the beam energy, contribute to decrease the final fragment charge.

Similar considerations can be applied also to the Z_R (and A_R) distributions for residue events shown in Fig. 5 panels (a) and (b), where the same hierarchy found for Z_{HF} and Z_{LF} [and also for Z_{BU} and A_{BU}, panels (c) and (d) of Fig. 5] is observed; in this figure only events in which all the involved fragments are identified both in charge and in mass are included; for the BU channel this corresponds to 63%, 82%, and 69% of all the BU events for the three reactions, respectively, while for the R channel this corresponds to 73% for the ^{40}Ca case and to 88% for both the ^{48}Ca beams, of all the residue events. The average values obtained for Z_{BU}, A_{BU}, Z_R, and A_R are reported in Table II. Both the average values of the table and the distributions of Fig. 5 show that the reconstructed fragments in the BU case are heavier than the residue ones for a given reaction. This may indicate that in case of BU part of the available excitation energy is exploited for the breakup process,[1] thus reducing the deexcitation chain, or that the breakup

---

[1]On the basis of the obtained fragment distributions, we can estimate that typical Q_{values} for the splitting are of the order of -25 MeV.
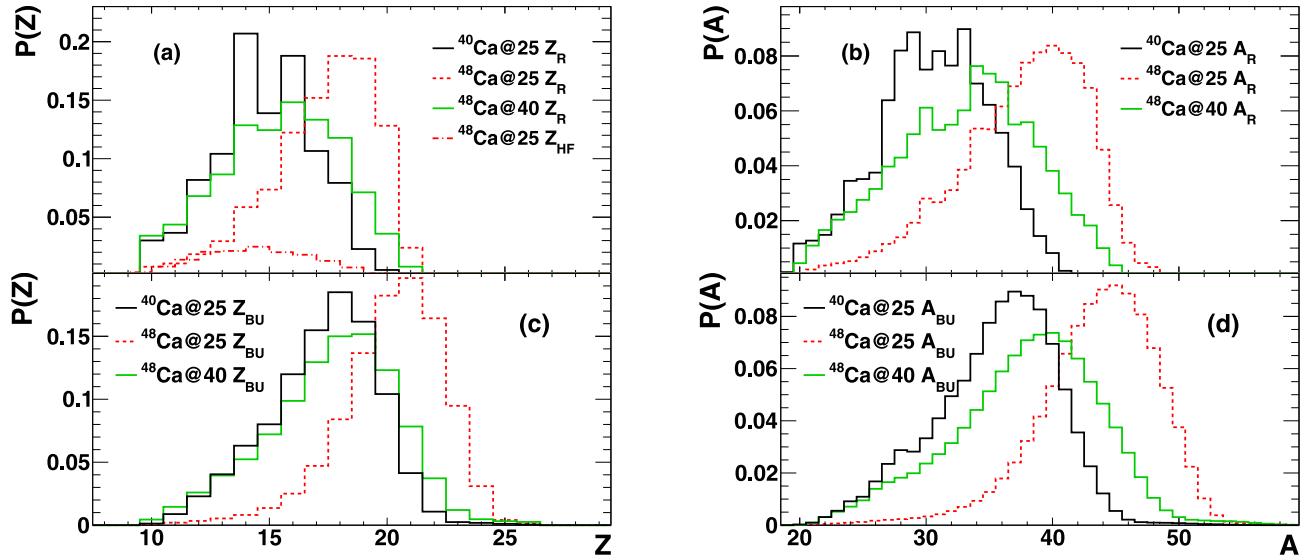
FIG. 5. (a) Relative probability distribution of Z_R for all the systems. Only the subset of events for which the mass of the heavy ejectile is detected is shown. Dash-dotted histogram: Z_{HF} distribution. (b) Relative probability distribution of mass (A_R) for the same fragments of panel (a). (c) Relative probability distribution of Z_{BU}. Only the subset of events for which the mass is experimentally detected for both fission fragments is shown. (d) Relative probability distribution of mass (A_{BU}) for the same events of panel (c).

process selects by itself heavier primary fragments. Due to the incomplete angular coverage of the setup, the Z_R distribution may include also HFs for which the LF has been lost; however, such a contribution, unavoidably present, is limited to the low-Z tail of the Z_R distribution, as shown in panel (a) by the red (light gray) dash-dotted line (corresponding to the Z_{HF} distribution for ^{48}Ca at 25 MeV/nucleon). In Table II we also present the average values of the charge and mass distributions obtained for simulated data, showing that the experimental hierarchy is reasonably reproduced by the simulation, with all the predicted values very close to the experimental ones.

The obtained results for the reactions at 25 MeV/nucleon concerning the scaling with the neutron richness of the system of both the BU asymmetry and the heaviest fragment size are fully compatible with the results on Ca+Ca,Ti reactions at the same energy reported in [33], although not exactly comparable; indeed, the neutron richness of the system allows for the formation of heavier fragments that, in case of BU, produce more asymmetric splits.

In Fig. 6 we show Z_{BU} vs the reconstructed c.m. velocity of the BU fragment[2] for the reaction ^{48}Ca + ^{12}C at 25 MeV/nucleon, when both fragments are isotopically identified; the velocity of the reconstructed nucleus lies in between that of the c.m. and that of the projectile (arrow position), closer to the former, signaling a strong degree of dissipation. This is similar to what can be recognized in Fig. 2(a), where heavy residues have laboratory velocities between the c.m. and the beam velocity; to better illustrate this point, in the inset of Fig. 6 we show the c.m. velocity distribution of all the BUFs as a continuous histogram, together with the c.m. velocity of the biggest fragment of the event, both for the class $Z \geqslant 10$ (dashed histogram) and for the specific channel $Z = 19$–20 (dotted histogram). The distribution of the detected biggest fragment with $Z \geqslant 10$ is rather broad and slightly shifted to velocities higher than that obtained for the BUF, thus signaling that a larger degree of dissipation is associated

———

[2]That is, the c.m. velocity of the center of mass of HF and LF.

TABLE II. Average charge and mass values for the measured heavy fragment in residue events (R) and for the reconstructed nucleus (obtained adding Z_{LF} and Z_{HF} for the charge and A_{LF} and A_{HF} for the mass) in BU events (BU), for both experimental and simulated data.

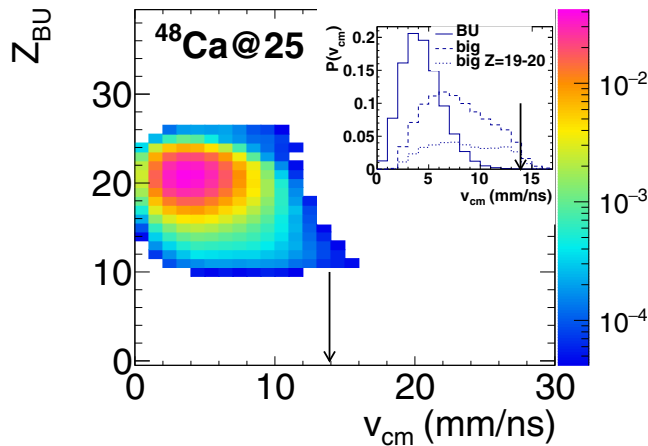| Projectile	Energy (MeV/nucleon)	Average Z_{BU}		Average Z_R		Average A_{BU}		Average A_R	
		Expt.	Sim.	Expt.	Sim.	Expt.	Sim.	Expt.	Sim.
^{40}Ca	25	17.2 ± 0.4	16.8 ± 0.4	14.8 ± 0.4	15.0 ± 0.5	35.5 ± 0.9	34.4 ± 0.9	30.6 ± 0.9	31.0 ± 1.0
^{48}Ca	25	20.2 ± 0.4	19.8 ± 0.4	17.3 ± 0.4	17.0 ± 0.4	43.6 ± 0.8	42.5 ± 0.9	37.5 ± 0.9	36.5 ± 0.9
^{48}Ca	40	17.7 ± 0.4	17.0 ± 0.4	15.4 ± 0.4	15.7 ± 0.5	37.9 ± 0.9	36.5 ± 0.8	33.0 ± 0.9	33.5 ± 0.9

FIG. 6. Z_{BU} vs $v_{c.m.}$ plot (reconstructed from the two breakup fragments) for the system ^{48}Ca at 25 MeV/nucleon. The arrow corresponds to the beam velocity. In the inset the projection on the $v_{c.m.}$ axis (continuous histogram) is shown, together with the c.m. velocity distribution of the biggest fragment of the event with $Z \geqslant 10$ (dashed histogram) and with $Z = 19$–20 (dotted histogram); distributions are normalized to their integral.

FIG. 7. Average N/Z as a function of Z; open symbols denote reconstructed BU fragment, full symbols R fragment. Dashed and continuous lines refer to reconstructed QP_{BU} and QP_R, respectively, from the data set of [9]. The dash-dotted black line represents the EAL prediction (average N/Z after statistical evaporation). Statistical errors are within the symbol size.

with the BU process. Moreover, as expected, when the charge of the biggest fragment is close to the projectile one, there is also a contribution in the region of the projectile velocity, associated with peripheral reactions, altogether lacking in the BU case. Therefore, it is quite reasonable to conclude that the candidate BU fragments are indeed compatible with a breakup process occurring after a very dissipative collision producing an incomplete fused system or an excited QP. In this respect we mention that the systematics [34] predicts for our systems a relative abundance of 15–17% at 25 MeV/nucleon and around 8% at 40 MeV/nucleon for the fusion channel.

2. Isotopic composition of the BU fragments

We now discuss the isotopic content of the BUFs, also in comparison with that of the R fragment. The average N/Z values are shown in Fig. 7 as a function of the charge for the three reactions. Two main observations can be given. The first one, concerning the neutron content of the beams, is the expected big gap separating the neutron-rich reactions from the $N = Z$ one; the N/Z gap is around 0.1, corresponding at $Z = 20$ to a difference of two neutrons. The n-rich cases are essentially above the N/Z, corresponding to the evaporation attractor line (EAL) [35] (dash-dotted black line in the figure), while the ^{40}Ca one is below that line. Assuming that the EAL line cannot be crossed during the statistical deexcitation phase, this could be interpreted as a sign that, independently of the dynamics of the reaction, the primary fragment population tends to remain on the same side of the EAL as the entrance channel.

A second comment concerns the beam energy: for the ^{48}Ca beam, the average N/Z is larger for the 25 MeV/nucleon reaction than for the 40 MeV/nucleon one.

Considering the two channels [i.e., BU (open symbols) or single heavy residue (full symbols)], the differences are small.
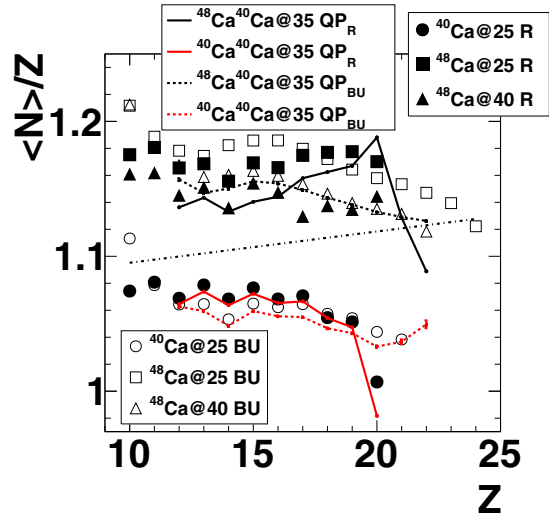
However, the BU fragments are slightly more neutron rich for $Z < 18$ for the ^{48}Ca projectile and slightly less neutron rich for the ^{40}Ca projectile with respect to the R fragments. The region beyond the projectile is not populated in the R case, while it is accessed by summing HF and LF in the BU channel.

The previous observations can be qualitatively understood by taking into account that, for primary sources with similar initial values of N and Z, larger excitations and thus longer evaporation chains lead closer to the EAL, which is approached by opposite injection points in the N-Z map for the two Ca beams. Thus, also the slight N/Z differences shown in the two channels (BU and R) might signal, on average, shorter evaporation chains for the BU channel due to the energy consumed by the splitting process. The net average N/Z decrease (and the consequent closer approach to the EAL) when the beam energy increases for the ^{48}Ca reactions can again reflect the average larger excitation energies at 40 MeV/nucleon (triangles vs squares) but an additional contribution from preequilibrium (neutron richer) emissions cannot be ruled out.

Figure 7 also contains the average N/Z values of quasiprojectile residues detected as such (QP_R, continuous lines) or reconstructed after breakup adding charge and mass of the two scission fragments (QP_{BU}, dashed lines), measured in ^{48}Ca + ^{40}Ca and ^{40}Ca + ^{40}Ca collisions at 35 MeV/nucleon coming from the data set investigated in [9]. It is important to note that since the Ca+Ca case corresponds to symmetric or near symmetric reactions, it is easy to select the QP source, at variance with what happens for the Ca+C case. Therefore we can now compare the average N/Z obtained for the QP of the Ca+Ca systems with the results for Ca+C, keeping in mind that in the latter case we are dealing with very damped events,

where QP and incomplete fusion are not easily distinguishable.

For ^{40}Ca beams, where the N/Z of the whole system and of the reaction partners separately is 1, the $\langle N \rangle / Z$ of the symmetric and asymmetric reactions are similar both for the BU/QP$_{BU}$ channel [dashed red (light gray) line and open circles] and for the R/QP$_R$ one [continuous red (light gray) line and full circles].

For ^{48}Ca beams the situation is less clear, because in this case the N/Z values of the whole system are different for the two datasets (1.2 for ^{48}Ca + ^{12}C and 1.3 for ^{48}Ca + ^{40}Ca). It is evident that the Ca+Ca results (black continuous and dashed lines) at 35 MeV/nucleon are closer to the Ca+C reaction at 40 MeV/nucleon (triangles), as reasonably expected. In the R channel the effect of peripheral collisions in the Ca+Ca case (continuous black line) pushes up the average N/Z towards the projectile value for Z close to 20, at variance with what happens for the Ca+C (full triangles), where such reactions are suppressed by the setup geometry. Instead, far from the peripheral region, for the QP$_R$/R channel the $\langle N \rangle / Z$ is almost independent of the target (^{40}Ca or ^{12}C). A possible explanation of this observation may be related to the isospin diffusion for the ^{48}Ca + ^{40}Ca case, which tends to shift the average N/Z of the QP towards the value of the whole ^{48}Ca + ^{12}C system.

3. The relative velocities of BU pairs

We now move on to investigate an important observable of the BU process, namely the relative velocity of the split partners. As a baseline we expect a phenomenon mainly ruled by the Coulomb repulsion, where the asymptotic relative velocity should be described by the Viola systematics for fission [36–38], although dynamical effects may give additional contributions [4,5]. For the following discussion we introduce upper and lower limits on Z_{BU}, in order to exclude on the one hand very small reconstructed parent nuclei missing a large part of the available charge and on the other the small tail of very big reconstructed fragments, corresponding to spurious events. Therefore we adopt $Z_{BU} > 13$ (corresponding to more than 50% of the total charge of the entrance channel) as lower limit for all the systems; on the basis of the distributions of Fig. 5(c), we choose as upper limits $Z_{BU} = 24, 22$ for the reactions with ^{48}Ca at 25 MeV/nucleon and at 40 MeV/nucleon, respectively, and $Z_{BU} = 21$ for the ^{40}Ca case.

The $\vartheta_{rel}^{c.m.}$ vs v_{rel} correlation (where $\vartheta_{rel}^{c.m.}$ is the relative angle in the c.m. frame between the two detected fragments and v_{rel} is their relative velocity) for HF and LF is shown in Figs. 8(a) and 8(b) for the two reactions ^{48}Ca + ^{12}C at both beam energies; in the panels (c) and (d) the corresponding relative velocity distributions are drawn. The correlations confirm that the maximum yield is compatible with BU from very damped events: indeed, most fragments are emitted at large relative angles (essentially back to back) as expected from a source close to $v_{c.m.}$. A tail extends to narrower relative angles, being more intense at the highest beam energy; this probably corresponds to BU sources for less dissipative events, flying at higher velocities, i.e., maybe coming from the QP breakup (for example, at 40 MeV/nucleon, the average value of the c.m. velocity of reconstructed BUF is 40% smaller for $\vartheta_{rel}^{c.m.}$
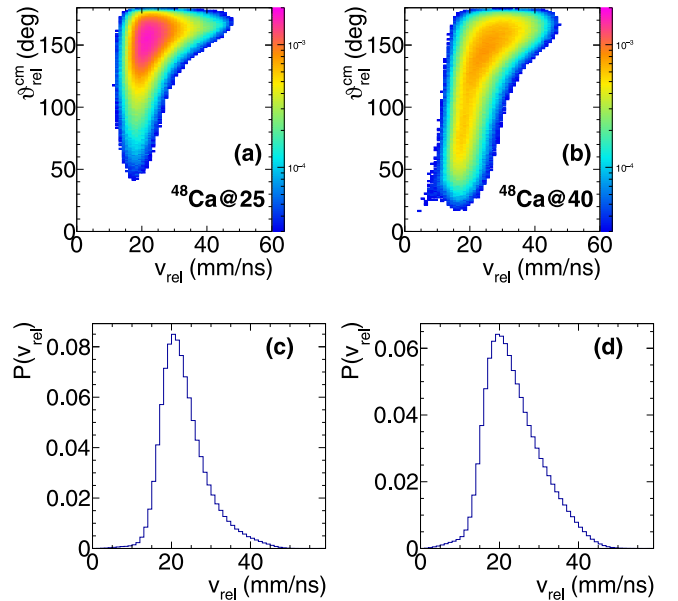

FIG. 8. Top: $\vartheta_{rel}^{c.m.}$ vs v_{rel} calculated for HF and LF. (a) ^{48}Ca at 25 MeV/nucleon. (b) ^{48}Ca at 40 MeV/nucleon. Bottom: Relative probability distribution of v_{rel} for the two reactions.

beyond $120°$ than below this limit). The different intensity of the tail at the two bombarding energies may be caused by the fact that at 40 MeV/nucleon the stronger kinematic focusing favors the BU detection even for c.m.-forward emitted sources (i.e., closer to the beam velocity).

We thus conclude that these correlations do not clearly point to different event types, but they confirm that we are dealing with a continuous and indistinct set of more or less hot primary sources, mostly close to $v_{c.m.}$ and likely heavier than the original projectile. In panels (c) and (d) of Fig. 8 the v_{rel} distributions are shown. At a first glance, we see that both distributions peak at the values predicted by the Viola formula [36]. For instance, if we consider the BU of a representative fragment ($Z_{BU} = 20$ and $A_{BU} = 44$, see Table II) with asymmetry 0.3, the Viola formula gives $v_{rel} = 20.0$ mm/ns, very close to the maximum of the distributions.

A more detailed analysis of the relative velocity of HF and LF and its comparison with the fission systematics can be attempted by fully exploiting the isotopic identification of both fission partners. For sake of clarity from now on we will consider only BU events with $\vartheta_{rel}^{c.m.} > 120°$, corresponding to the most dissipative reactions.

Recall that the Viola systematics describes the average kinetic energy E_K of fission fragments in Coulomb driven breakup. The systematics, initially published for heavy nuclei where the fission process is more probable, was then extended to medium mass sources. The formula gives only one value of E_K for a parent nucleus with mass A and charge Z, independently of the breakup asymmetry [36]: $E_K = 0.1189 Z^2 / A^{1/3} + 7.3$ MeV. From E_K the relative velocity of the fragments can be obtained if both their masses are known. In some published data for which the expected velocity for the Coulomb breakup is calculated, the two fragments
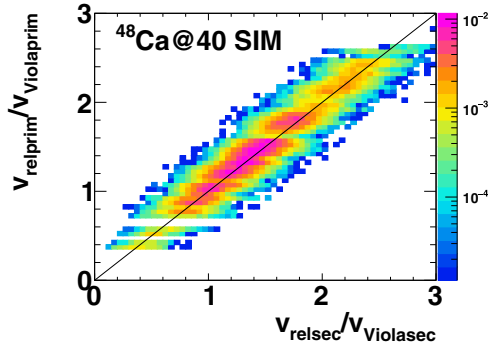
FIG. 9. AMD(+GEMINI++) predictions for the reaction at 40 MeV/nucleon: ratio of the relative velocity calculated at 500 fm/c to the Viola velocity (calculated with masses and charges at 500 fm/c) vs ratio of the secondary relative velocity (after the afterburner) to the Viola velocity calculated with secondary masses and charges for BU events.

are identified in charge [38] and a hypothesis on the mass[3] is needed to obtain the relative velocity. In other cases [39] when measuring masses from kinematic methods (e.g., from kinetic energy and time of flight), it is necessary to guess the primary charge to derive the expected relative velocity from E_K.[4] In this work, instead, the fragments coming from the breakup can be both isotopically identified; therefore, at least for this subset of events, it is possible to calculate the E_K given by the Viola formula using the experimentally measured Z_{BU} and A_{BU} on an event by event basis[5] and the passage from E_K to relative velocity does not introduce additional hypotheses.

Nevertheless, we should note that since we calculate the Viola velocity (v_{Viola}) by means of quantities relative to measured (secondary) fragments, some effects due to the evaporation from the reseparating pair (after the split) might be present. However, we argue that this effect should be small because for the nuclei under study the splitting process dissipates a considerable amount of energy (all the breakup reactions are endoenergetic in this region of masses).

In fact, within the AMD+GEMINI++ model, we have checked this assumption: we verified using the simulated data that when the breakup takes place before 500 fm/c (i.e., during the dynamical calculation), the ratio of the relative velocity obtained at such a time to v_{Viola} calculated with masses and charges at 500 fm/c is on average equal to that calculated after the evaporation using secondary quantities, as shown in Fig. 9.

Thanks to the knowledge of mass and charge of both fission fragments, we can check the effect of estimating the breakup

---

[3]In [38] $A_i = 2.08Z_i + 2.9 \times 10^{-3}Z_i^2$, where $Z_{i=1,2}$ is the charge of the breakup pair; moreover the relative kinetic energy is calculated as $E_{rel} = [1.44Z_1Z_2/r_0(A_1^{1/3} + A_2^{1/3}) + 2.0]$ MeV with r_0 obtained equating E_{rel} to E_K of [36] in the hypothesis of symmetric split.

[4]In this case the authors explicitly introduce the split asymmetry in the calculation of the relative energy: $E_K = [0.755Z_1Z_2/(A_1^{1/3} + A_2^{1/3}) + 7.3]$ MeV.

[5]That is, $E_K = [(0.1189)(Z_{HF} + Z_{LF})^2/(A_{HF}+A_{LF})^{1/3} + 7.3]$ MeV.
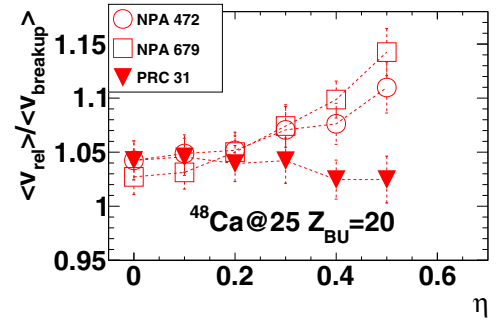

FIG. 10. Average relative velocity between the breakup fragments normalized to the average velocity reported in [38] (NPA679), [39] (NPA472), and [36] (PRC31) as a function of the charge asymmetry for $Z_{BU} = 20$ and for the system ^{48}Ca at 25 MeV/nucleon.

velocity due to the Coulomb repulsion using the Viola formula of [36] and the full experimental information (i.e., Z_{HF}, Z_{LF}, A_{HF}, and A_{LF}) or using only partial information (only Z and the prescription of [38]) and/or different formulas proposed in the literature (the formula of [39] with experimental charges and masses). The result is shown in Fig. 10 as a ratio between the experimental relative velocity and the calculated ones for $Z_{BU} = 20$, exploiting the experimental data coming from the ^{48}Ca low energy reaction. When the Viola prescription and the full experimental information are used, the obtained ratio, although greater than 1, is almost independent of the charge asymmetry. In contrast, when other prescriptions and/or partial information are used, the ratio is similar to that obtained in the previous case at small charge asymmetries, while it significantly deviates from it beyond $\eta = 0.3$. Therefore the use of these recipes to estimate the breakup velocity associated with the Coulomb repulsion, as for example in [4], where [39] is used, may produce a distortion at large asymmetries. As a consequence in the following discussion the experimental relative velocities will be compared to those given by the Viola prescription [36] keeping only the events in which both breakup fragments are isotopically identified.

Figure 11 displays the relative velocity normalized to v_{Viola} for the three studied reactions as a function of the charge asymmetry and for some different Z_{BU} values. For all systems the obtained ratio is almost independent of Z_{BU} (the not shown cases are very similar to the displayed ones) and η; concerning the evolution with the beam energy, a clear increase was observed moving from the systems at 25 MeV/nucleon (for which all the ratio values are between 1.04 and 1.08 for the ^{40}Ca beam and between 1.00 and 1.06 for ^{48}Ca) to that at 40 MeV/nucleon (where the ratios are in the range 1.13–1.20).

This finding suggests the occurrence of some additional contributions (beyond Coulomb repulsion) acting during the breakup process, whose weight increases with the beam energy; possible explanations of this effect might be the larger angular momentum of the system attained during the evolution of the dynamical phase and/or a more stretched phase space configuration of the breaking source.

Concerning the angular momentum, a rough calculation indicates that the ratio $\mathcal{R}$ of the relative velocity between HF and LF and the velocity due to Coulomb repulsion (calculated
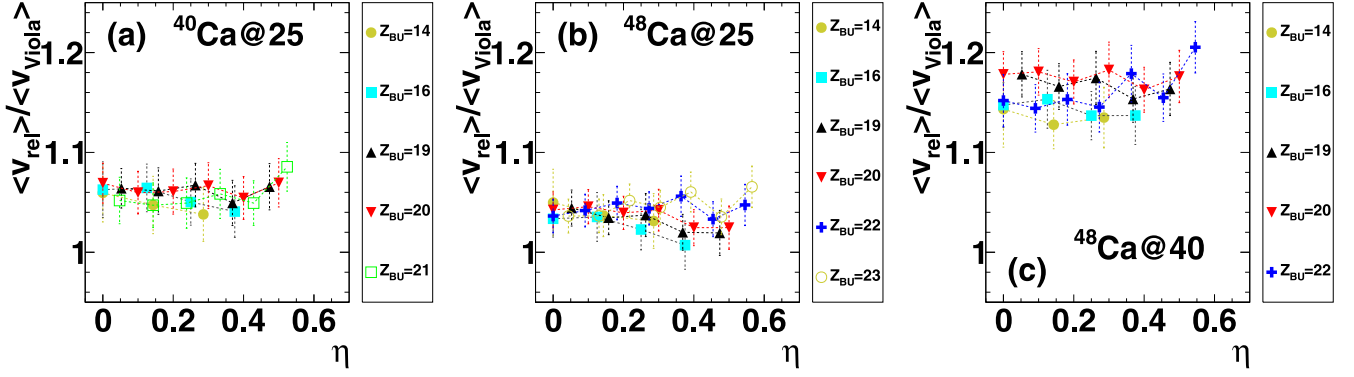
FIG. 11. Average relative velocity between HF and LF normalized to the average v_{Viola} [36] as a function of the charge asymmetry; each symbol/color corresponds to reconstructed fragments with charge $Z_{\text{BU}} = Z_{\text{HF}} + Z_{\text{LF}}$. Each panel shows a different system.

from $E_{\text{Coul}} = 1.44 \frac{Z_{\text{HF}} Z_{\text{LF}}}{(1.2 A_{\text{HF}}^{1/3} + 1.2 A_{\text{LF}}^{1/3})}$ MeV) should depend on the angular momentum of the system according to the formula $\mathcal{R} = \sqrt{1 + \frac{E_{\text{rot}}}{E_{\text{Coul}}}}$, where $E_{\text{rot}} = \frac{L^2}{2I}$ is the rotational energy. In this formula L is the angular momentum and I is the moment of inertia calculated for two rigid spheres (corresponding to the BU fragments) in contact with respect to a perpendicular axis passing through their c.m.[6] Figure 12 shows the expected ratio $\mathcal{R}$ as a function of η for different values of L for $Z_{\text{BU}} = 20$. For $L = 0$ the ratio is exactly 1 by construction and it grows about 4–5% for an increase of $20\hbar$. Therefore, if we suppose that the average angular momentum of the fragmenting system increases with the beam energy, we can expect an increase of the $v_{\text{rel}}/v_{\text{Viola}}$ ratio.

Although the AMD simulation does not guarantee angular momentum conservation if not purposely forced [10], we have verified that within this model the hypothesis that the average angular momentum of the breaking up fragment increases with the beam energy is not supported. In fact for all the simu-

---

[6]$I = \frac{2}{5}[A_{\text{HF}}(1.2 A_{\text{HF}}^{1/3})^2 + A_{\text{LF}}(1.2 A_{\text{LF}}^{1/3})^2] + A_{\text{red}}(1.2 A_{\text{HF}}^{1/3} + 1.2 A_{\text{LF}}^{1/3})^2$, where $A_{\text{red}} = \frac{A_{\text{HF}} A_{\text{LF}}}{(A_{\text{HF}} + A_{\text{LF}})}$.

lated reactions the spin distributions of the primary fragments just before the breakup taking place during the dynamical phase are very similar and have average values below $20\hbar$.

Nevertheless, the simulation AMD+GEMINI++ still predicts an increase of the $v_{\text{rel}}/v_{\text{Viola}}$ ratio with the beam energy (variation of the order of 20% from 25 MeV/nucleon to 40 MeV/nucleon) as in the experimental case, as shown in Fig. 13 for some Z_{BU}, although in this case a systematic decrease of the ratio for all Z_{BU} when η increases appears, at variance with the experimental data; moreover, the ratio at 25 MeV/nucleon is always below 1.

Looking at the whole $v_{\text{rel}}/v_{\text{Viola}}$ distribution it is possible to put into evidence that both in the experimental and in the simulated case the difference in the average value between 25 and 40 MeV/nucleon is mainly due to a tail extending towards high values in the case of the high energy beam; this behavior may reflect the fact that at 40 MeV/nucleon the breaking up fragment is more stretched due to dynamical effects, i.e., it has a more elongated shape (in velocity) due to a stronger memory of the entrance channel. As a support of this hypothesis we verified that in the model the velocity distribution along the beam axis of the single nucleons forming the fragment just before the breakup is broader at 40 MeV/nucleon than at 25 MeV/nucleon.
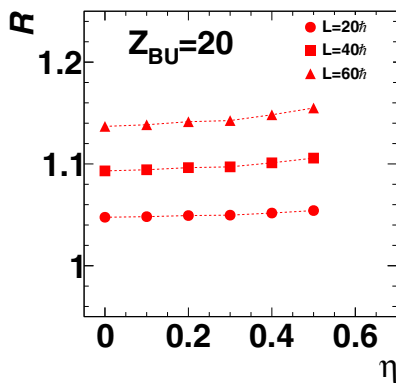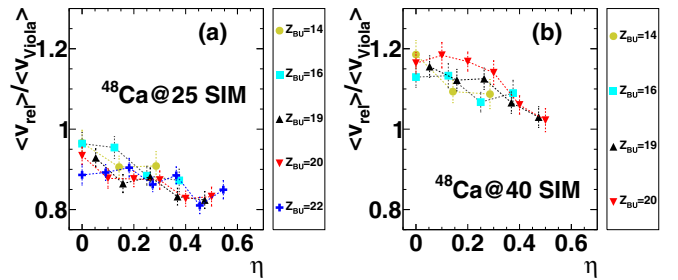

FIG. 12. $\mathcal{R} = \sqrt{1 + \frac{E_{\text{rot}}}{E_{\text{Coul}}}}$ calculated for different values of angular momentum of the breaking up system as a function of η for $Z_{\text{BU}} = 20$.

FIG. 13. Simulated data (AMD+GEMINI++): average relative velocity between HF and LF normalized to the average v_{Viola} as a function of the charge asymmetry; each symbol/color corresponds to a different Z_{BU} (same legend as in Fig. 11). Each panel shows a different system.

These results suggest the interpretation of the trend observed in Figs. 11(b) and 11(c) in terms of an increasing weight of dynamical effects. Despite such a contribution, relative velocity distributions located close to the values coming from the fission systematics are a signature of a basically Coulomb-driven breakup. Therefore in the following we will use such an observable as a probe of the fact that also a fragment reconstructed via particle correlation and detected in coincidence with a heavier one in many cases can be interpreted as the LF of a breakup process.

4. Breakup channel with the light fragment reconstructed via particle fragment correlations

In the BU process the excitation energy of the splitting fragment can be high enough to allow for further particle decay. In particular if the LF is produced in an excited state decaying via particle emission and if its decay products are detected in coincidence, the LF can be reconstructed by means of the particle-particle correlation technique.

The correlation technique has been widely used in the literature to investigate the emission source size and/or the emission time [40,41]. In this paper we mainly restrict the analysis to the resonances of C isotopes decaying in channels including the emission of α particles since they are collected with high statistics. The technique basically consists of selecting events where two particles (labeled as 1 and 2), candidates to be the decay products of a parent resonance, are detected. We build the observable $1 + R(E_{rel}) = C \frac{\sum Y_{12}(\vec{p}_1, \vec{p}_2)}{\sum Y_{12}^{unc}(\vec{p}_1, \vec{p}_2)}$, where $Y_{12}(\vec{p}_1, \vec{p}_2)$ are the correlated yields of the pair (i.e., the pairs are detected in the same event) and $\vec{p}_i$ with $i = 1, 2$ is the particle momentum, while $Y_{12}^{unc}(\vec{p}_1, \vec{p}_2)$ are the uncorrelated ones, estimated by means of the event mixing technique [42]. The summations run over pairs of momenta $\vec{p}_1$ and $\vec{p}_2$ corresponding to the same value of relative energy E_{rel}, where $E_{rel} = (\vec{p}_1 - \vec{p}_2)^2/2\mu$, with μ the reduced mass of the pair. C is a normalization coefficient estimated at large E_{rel} with the condition $R(E_{rel}) \rightarrow 0$. The building of the uncorrelated yields is a critical procedure which should take into account the efficiency of the setup for the different kinds of events, the event class selection (which should be the same both for the correlated and the uncorrelated case), and the conservation laws (which should be checked not to be violated for uncorrelated events, otherwise distortions can be produced) [43–45]. We also note that in the present case the previous issues for proper background evaluation are enhanced by the limited angular coverage of the apparatus which in addition differently affects the efficiency for the reactions at 25 and 40 MeV/nucleon. Therefore the following analysis is focused on showing that the emission pattern of the reconstructed fragments is compatible with that of the LF in BU events, without attempting quantitative analysis on the population of the different levels, also because many of them are not resolved. In fact the setup is mainly limited by the angular resolution of the telescopes ($\Delta\vartheta$ around $1.26°$ in the adopted configuration, where ϑ is the polar angle) and to a lesser extent by the energy resolution (around 0.1 MeV). More quantitative studies on particle-particle correlations may be the subject of future investigations with the complete setup INDRA-FAZIA,
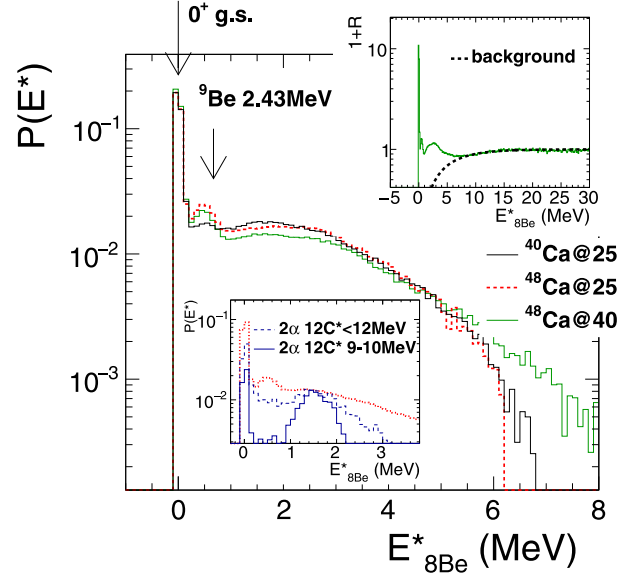

FIG. 14. Relative probability distribution of the excitation energy of ^{8}Be* reconstructed from two-α correlations, after background subtraction. In the top inset $1 + R(E^*)$ vs E^* for ^{48}Ca at 40 MeV/nucleon is shown as green (gray) line; the black dashed line is the Coulomb background. Bottom inset: relative probability distribution of the ^{8}Be* excitation energy spectrum without background subtraction for the system ^{48}Ca at 25 MeV/nucleon [red (gray) dotted line]; dashed line: feeding from ^{12}C* with $E^* < 12$ MeV (details in the text). Continuous line: the same but with E^* of the ^{12}C* between 9 and 10 MeV. The normalization is done at 1.4 MeV.

where the topic of the energy and momentum conservation effects on the event mixing spectrum will be quantitatively faced thanks to the very high angular coverage of the device.

(a) ^{12}C*. Concerning ^{12}C, reconstructed through its decay into three α (particularly interesting as a test bench of clustering in nuclei [32,46,47]), we limit the analysis to the cases in which the decay is of sequential type (predominant for the Hoyle state [47,48]) and proceeds through the formation of ^{8}Be. This lighter cluster is reconstructed starting from two-α correlations; the obtained excitation energy spectra for the three reactions (after the Coulomb background subtraction), normalized to their integral to better compare the shapes, are shown in the main frame of Fig. 14. These spectra refer to all detected events with at least two α, without specific selections. In the top inset of Fig. 14 the $[1 + R(E^*)]$ vs E^* distribution,[7] which is the starting point used to extract the excitation energy spectrum, is drawn for the system at 40 MeV/nucleon; also shown in the plot is the Coulomb background, fitted in the smooth region $E^* \geqslant 20$ MeV according to the formula $y = 1 - e^{-E^*/E_c}$ [49] (E_c is the fit parameter).

The excitation energy spectra depicted in the main frame of Fig. 14 clearly show the narrow peak close to zero corresponding to the ground state of ^{8}Be (91 keV); a smaller
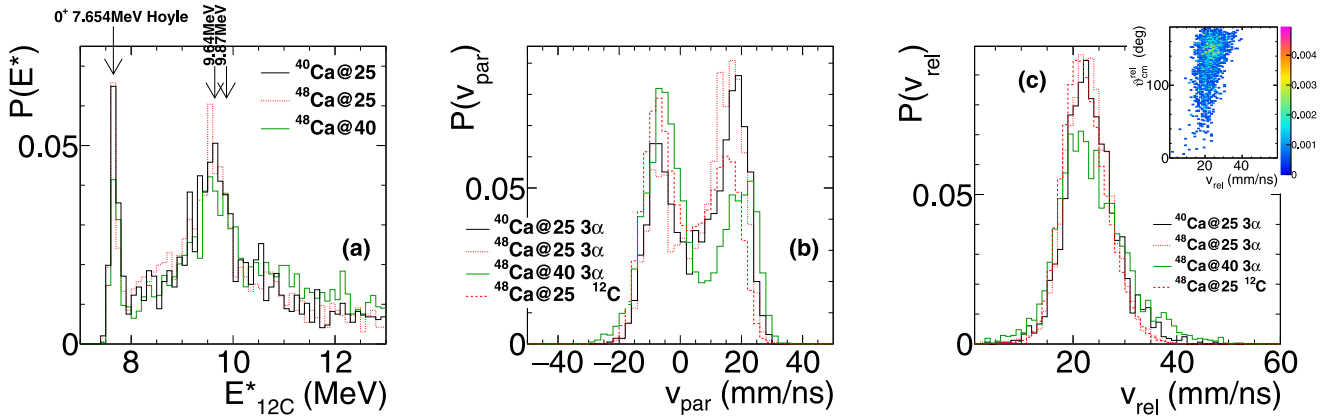
---

[7]$E^* = E_{rel} - Q_{value}$.

FIG. 15. (a) Relative probability distribution of the excitation energy of $^{12}C^*$ reconstructed from three-α correlations, two of them ascribed to ^{8}Be ground state, in events with $M_\alpha = 3$ and with a fragment with $Z \geqslant 10$ in coincidence. Neither background subtraction nor uncorrelated yield normalization was applied. Some relevant excited levels are marked with arrows. (b) Continuous and dotted histograms: relative probability distribution of the c.m. parallel velocity of the reconstructed $^{12}C^*$ calculated with respect to the velocity of the biggest fragment of the event, corrected for the correlated recoil, for $E^*_{12C} < 15$ MeV. Dashed histogram: the same but for the detected (cold) ^{12}C. (c) Continuous and dotted histograms: relative probability distribution of the relative velocity between the reconstructed $^{12}C^*$ and the big fragment, for $E^*_{12C} < 15$ MeV. Dashed histogram: the same but for the detected (cold) ^{12}C. In the inset is a plot of the relative c.m angle vs relative velocity between the $^{12}C^*$ and the big fragment for the system ^{48}Ca at 25 MeV/nucleon.

peak, more abundant for the ^{48}Ca systems, is located around 0.5 MeV. As discussed in the literature [50] it mainly corresponds to the incomplete reconstruction of the excited ^{9}Be (energy level[8] 2.43 MeV) for which the free neutron is not detected; it is reasonable that its contribution is larger for the neutron rich ^{48}Ca reactions; its population also decreases passing from 25 to 40 MeV/nucleon.[9] The presence of the second excited state 2^+ at 3.03 MeV of ^{8}Be is masked by the background due to incompletely reconstructed $^{12}C^*$ nuclei decaying into three α, as shown in the bottom inset of Fig. 14 for the system ^{48}Ca at 25 MeV/nucleon. In this plot the excitation energy of ^{8}Be without background subtraction [dotted red (gray) line] is presented for events with at least two α, together with the spectra obtained rejecting one α in events with three detected α and excitation energy of the $^{12}C^*$ [preconstructed as explained in the following and shown in Fig. 15(a)] in the region $E^* < 12$ MeV (dashed line) or for $9 < E^* < 10$ MeV (continuous line). As already shown in [51], this plot suggests that also the resonances of ^{12}C around 9–10 MeV tend to decay via the ^{8}Be, as the Hoyle state; in fact, rejecting one α, the ground state of the ^{8}Be is clearly populated.

From now on we gate on the ground state of ^{8}Be and we seek the coincidence with a heavy fragment ($Z \geqslant 10$). A third coincident α particle is then required and the excitation energy spectrum of $^{12}C^*$ shown in Fig. 15(a) is produced[10] for all the reactions (the histograms are normalized to their integral). In this case the exclusive requirements imposed to produce such a spectrum (a four-body channel: three α and a heavy fragment) strongly reduce the uncorrelated background; therefore it is not strictly necessary to divide for the uncorrelated yields and to subtract the background at least to give qualitative interpretation of these events. The spectra are very similar for the three reactions. The first narrow peak at 7.65 MeV is the Hoyle state; a broader peak clearly emerges below 10 MeV corresponding to known (unresolved) states around 9.6–10 MeV. In more detail the yield ratio of the highest energy peaks (between 8.85 and 10.25 MeV) to the Hoyle peak (between 7.45 and 7.95 MeV) shows a trend to increase with the beam energy (from 3.5 ± 0.3 for ^{48}Ca at 25 MeV/nucleon to 3.9 ± 0.4 for the same reaction at 40 MeV/nucleon), thus suggesting that higher excitations may be favored by larger beam energies. The neutron-poor system gives 3.1 ± 0.3, perhaps meaning that final states closer to the g.s. of ^{12}C can be favored in the $N = Z$ system.

The c.m. parallel velocity spectra of the reconstructed ^{12}C resonances, calculated with respect to the direction of the heaviest fragment of the event, are shown in Fig. 15(b) for $E^*_{12C} < 15$ MeV. For all the systems the distribution is almost symmetric with respect to the heavy fragment velocity, which is close to the c.m.; the two reactions at 25 MeV/nucleon

_____

[8]The obtained value around 0.5 MeV is slightly below the expected one of 0.67 MeV; the expected value is calculated from $E^* = E^*_{9Be} - Q_{9Be \to 8Be+n} - Q_{8Be \to \alpha+\alpha}$. This shift may be due to a deformation of the excitation energy spectrum caused by a defective production of the uncorrelated yields.

[9]The decay of ^{9}Be from the level at 1.68 MeV (with 100% probability of neutron decay) falls in the region of the ^{8}Be ground state and it cannot be resolved, thus acting as a further background for this state.

_____

[10]$E^*_{12C} = \sum_{i=1}^{3} E_i - Q_{12C \to 3\alpha}$, where E_i is the kinetic energy of the ith α calculated with respect to the c.m. of the three α.
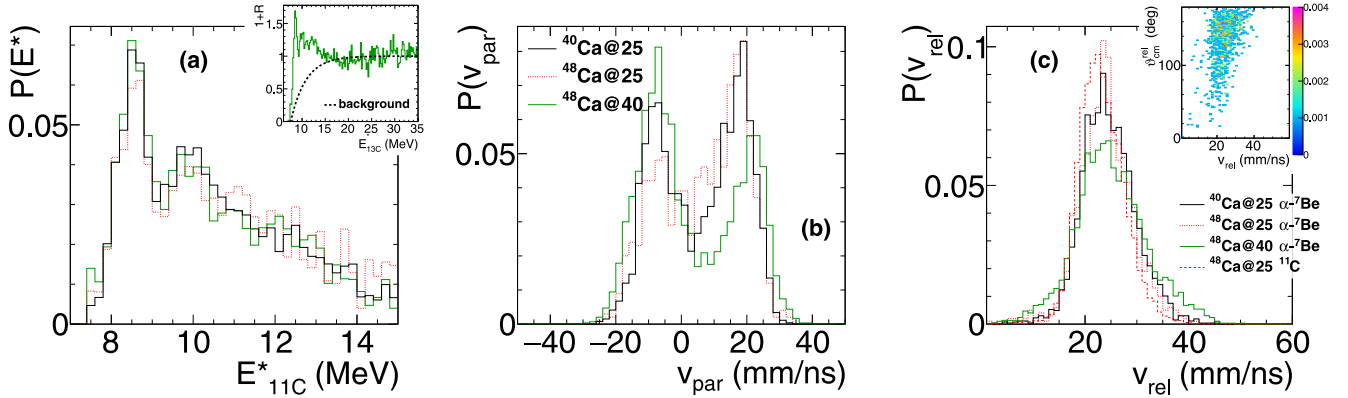
FIG. 16. (a) Relative probability distribution of the excitation energy of ^{11}C* reconstructed from α-^{7}Be correlations after background subtraction. In the inset the $1 + R$ distribution and the Coulomb background for ^{48}Ca at 40 MeV/nucleon are shown. (b) Relative probability distribution of the c.m. parallel velocity of the reconstructed ^{11}C* calculated with respect to the velocity of the biggest fragment of the event, corrected for the correlated recoil (for events in which a $Z \geqslant 10$ ejectile is detected in coincidence), for $E^*_{11C} < 15$ MeV. (c) Continuous and dotted histograms: relative probability distribution of the relative velocity between the c.m. of α and ^{7}Be and the biggest fragment of the event, for $E^*_{11C} < 15$ MeV. Dashed histogram: the same but for the detected ^{11}C. In the inset the relative c.m angle vs the relative velocity between the heavy fragment detected in coincidence and the c.m. of α and ^{7}Be for the system ^{48}Ca at 25 MeV/nucleon is shown.

produce very similar distributions, while for the high energy reaction the forward peak is slightly shifted towards higher velocities. Such an emission pattern is compatible with the presence of an almost fully damped source and, anyhow, it is similar to the parallel velocity distribution obtained when the ^{12}C is detected as such [dashed line in Fig. 15(b)]. The residual shape difference might be due to the efficiency variation for the detection of a ^{12}C as such and of three α in coincidence.

The coincidence between a carbon (detected or reconstructed) and an heavy fragment (playing the role of HF) belongs to the BU channel as defined in this work ($Z_{LF} \geqslant 5$); therefore it is worth looking at the relative velocity between the reconstructed ^{12}C* and the coincident heavy fragment]Fig. 15(c)]. The v_{rel} distribution obtained for all the reactions is compatible with a mainly Coulomb-driven breakup process with peak values around 21 mm/ns, in close similarity with the distribution of Fig. 8(c). Also the $\vartheta^{c.m.}_{rel}$ vs v_{rel} correlation, shown in the inset, remarkably looks like that of Fig. 8(a). For ^{48}Ca at 25 MeV/nucleon also the v_{rel} distribution obtained when the ^{12}C is detected as such is shown as red (gray) dashed line in the main frame and it turns out to be very similar to the reconstructed one [red (gray) dotted line].

(b) ^{11}C*. The correlation technique applied to ^{12}C can be extended to other carbon isotopes. In Fig. 16(a) the excitation energy spectrum of ^{11}C* reconstructed from the $\alpha + ^7$Be channel, after background subtraction, is shown for the three systems; for completeness, in the inset the $1 + R$ distribution together with the estimated Coulomb background is shown for the high energy reaction. Various structures corresponding to excited levels can be seen in this plot; for example the first corresponds to the level 8.654 MeV, with a 100% probability of α decay, but a contribution from the 8.42 MeV level, with a lower α decay probability, cannot be excluded. The peak region beyond 9.3 MeV and below 10.5 MeV corresponds to unresolved levels, not decaying only with α emission. Within the resolution of the present analysis and within the statistical

errors, the populations of the different levels result to be very similar for the three reactions. As a check of the reconstruction procedure, in addition to the α-^{7}Be correlation, in Fig. 17 we show the ^{11}C* states obtained through the p-^{10}B channel (dashed histogram, 40 MeV/nucleon reaction only). Within the limit of the present resolution we indeed find results coherent with the known level structure.

Figures 16(b) and 16(c) show the same distributions already built for the three-α case [Figs. 15(b) and 15(c)] for the system α-^{7}Be; the plots, normalized to the integral, are
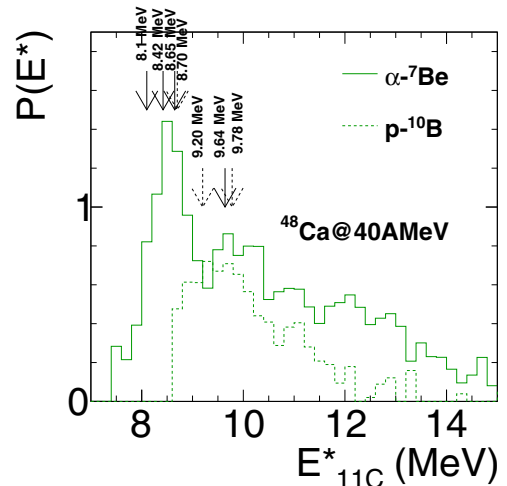

FIG. 17. Relative probability distributions of the excitation energy of ^{11}C* for the reaction ^{48}Ca at 40 MeV/nucleon obtained from two decay channels; the continuous histogram refers to the $\alpha + ^7$Be decay while the dashed histogram refers to $p + ^{10}$B. In both cases background was subtracted. Some tabulated excited levels are marked with arrows (dashed arrows for exclusive proton decaying levels).
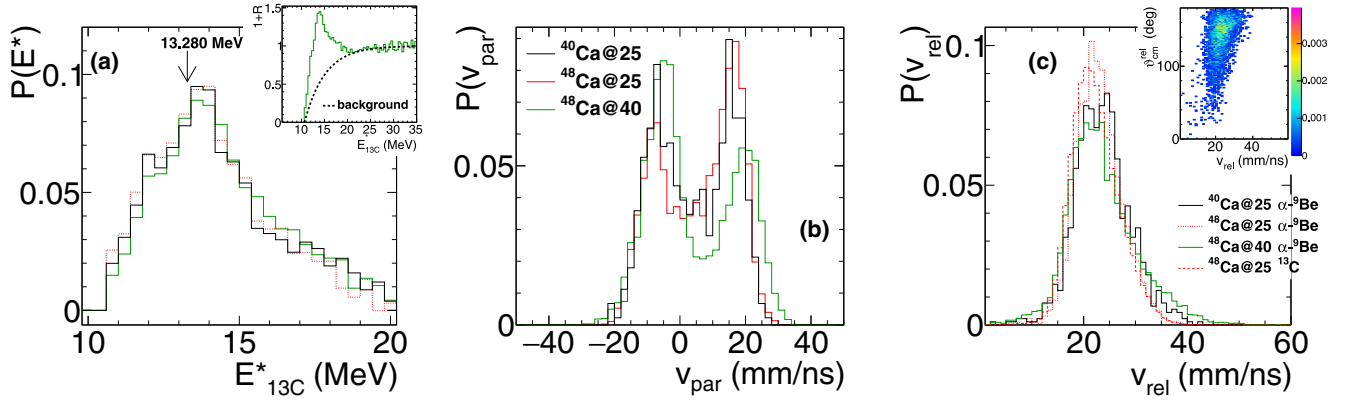
FIG. 18. (a) Relative probability distribution of the excitation energy of $^{13}C^*$ reconstructed from α-^{9}Be correlations after background subtraction. In the inset the $1 + R$ distribution and the Coulomb background for ^{48}Ca at 40 MeV/nucleon are shown. The only tabulated level reliably α decaying is marked with an arrow. (b) Relative probability distribution of the c.m. parallel velocity of the reconstructed $^{13}C^*$ calculated with respect to the velocity of the biggest fragment of the event with $Z \geqslant 10$, corrected for the correlated recoil, for $E^*_{13C} < 15$ MeV. (c) Continuous and dotted histograms: relative probability distribution of the relative velocity between the c.m. of α and ^{7}Be and the biggest fragment of the event, for $E^*_{13C} < 15$ MeV. Dashed histogram: the same but for the detected ^{13}C. In the inset the relative c.m angle vs the relative velocity between the heavy fragment detected in coincidence and the c.m. of α and ^{9}Be for the system ^{48}Ca at 25 MeV/nucleon is shown.

obtained requiring the coincident $Z \geqslant 10$ fragment and with the gate $E^*_{11C} < 15$ MeV. The spectra for ^{11}C resonances are overall very similar to those obtained for ^{12}C states; also in this case the background contribution is small due to the fact that we are gating on a three-body coincidence between α, ^{7}Be, and a fragment with $Z \geqslant 10$. In conclusion, the velocity patterns [panels (b) and (c)] confirm that in the examined events the ^{11}C (detected or reconstructed) is the LF of the breakup process of a heavier source.

(c) $^{13}C^*$. Finally, we apply the same analysis to the *n*-rich $^{13}C^*$ resonances, showing the results in the same manner as before in Fig. 18. Quite similar conclusions about the breakup origin of these resonances can be drawn by inspecting these panels. As for the excitation spectrum [panel (a)] we note again the remarkable similarity of the three reactions. Moreover, the details of the excited levels of $^{13}C^*$ are less known [52]; only one α decaying level with 100% probability and width of 340 keV is tabulated (around 13.28 MeV; the energy is slightly uncertain). Other levels that are candidates for α decay are known, but the probability is undefined. The reconstructed energy spectrum (after background subtraction) for $^{13}C^*$ is therefore interesting and is overall compatible with the partially known structure. Panels (b) and (c) of Fig. 18 lead to analogous conclusions about the origin of the ^{13}C, either produced beyond or below the particle separation energy: namely, the findings strongly support that the emission pattern of the reconstructed $^{13}C^*$ is compatible with a breakup process from either an incomplete fusion source or from very dissipative collisions.

IV. SUMMARY AND CONCLUSONS

In this work, we discussed experimental data for the asymmetric reactions ^{40,48}Ca + ^{12}C at 25 MeV/nucleon and ^{48}Ca + ^{12}C at 40 MeV/nucleon, collected with six blocks of the FAZIA setup. The data set mainly corresponds to

both incomplete fusion and strongly damped binary collisions which produce various primary nuclei, possibly deformed and with broad excitation energy distributions, that may undergo a breakup process. The analysis focused on some features of the breakup events which have been investigated with unprecedented detail thanks to the excellent isotopic separation achieved with the FAZIA telescopes (up to $Z \approx 25$). After a general characterization of BU events from the point of view of the charge asymmetry, of the size of the fragments and of their isotopic composition, the relative velocity between the breakup fragments was accurately studied and discussed in comparison with the predictions of the low-energy Coulomb-driven systematics for fission, taking into account the measured charge and mass of both HF and LF. A growth of the v_{rel} to v_{Viola} ratio with the beam energy was observed, perhaps related to stronger dynamical effects.

If the light fragment coming from the BU is excited beyond particle separation energy, it is possible to reconstruct the LF by means of the particle correlation, as was shown for some carbon isotopes on exclusive many body events. To our knowledge, a similar analysis on the BU channel is not present in the literature. The obtained emission pattern and in particular the relative velocity between the reconstructed LF and the detected HF turned out to be very similar to the case in which the carbon isotope was detected as such.

It is our intention to extend the analysis of the BU channel to other available data sets. For example, the case of the light asymmetric systems ^{32}S, ^{20}Ne + ^{12}C at 25 and 50 MeV/nucleon [28] may allow for the investigation of sources produced through very damped collisions (as in this case) but with smaller sizes, with possible effects on the relative velocity. The QP breakup will be instead investigated on the almost symmetric systems ^{58,64}Ni + ^{58,64}Ni at 32 and 52 MeV/nucleon [29], taking advantage of the high degree of completeness of these data, which where collected with the INDRA FAZIA setup.

[1] G. Casini, P. G. Bizzeti, P. R. Maurenzig, A. Olmi, A. A. Stefanini, J. P. Wessels, R. J. Charity, R. Freifelder, A. Gobbi, N. Herrmann, K. D. Hildenbrand, and H. Stelzer, Phys. Rev. Lett. **71**, 2567 (1993).

[2] L. Gingras, A. Chernomoretz, Y. Larochelle, Z. Y. He, L. Beaulieu, G. C. Ball, F. Grenier, D. Horn, R. Roy, M. Samri, C. St-Pierre, D. Thériault, and S. Turbide, Phys. Rev. C **65**, 061604(R) (2002).

[3] E. D. Filippo, A. Pagano, E. Piasecki, F. Amorini, A. Anzalone, L. Auditore, V. Baran, I. Berceanu, J. Blicharska, J. Brzychczyk *et al.* (REVERSE Collaboration), Phys. Rev. C **71**, 064604 (2005).

[4] E. De Filippo *et al.*, Phys. Rev. C **86**, 014610 (2012).

[5] E. De Filippo and A. Pagano, Eur. Phys. J. A **50**, 32 (2014).

[6] A. Jedele, A. B. McIntosh, K. Hagel, M. Huang, L. Heilborn, Z. Kohley, L. W. May, E. McCleskey, M. Youngs, A. Zarrella, and S. J. Yennello, Phys. Rev. Lett. **118**, 062501 (2017).

[7] A. Rodriguez Manso, A. B. McIntosh, A. Jedele, K. Hagel, L. Heilborn, Z. Kohley, L. W. May, A. Zarrella, and S. J. Yennello, Phys. Rev. C **95**, 044604 (2017).

[8] A. Hannaman, A. B. McIntosh, A. Jedele, A. Abbott, J. Gauthier, K. Hagel, B. Harvey, Z. Kohley, Y. Lui, L. A. McIntosh, A. R. Manso, M. Sorensen, Z. Tobin, R. Wada, M. Youngs, and S. J. Yennello, Phys. Rev. C **101**, 034605 (2020).

[9] A. Camaiani, G. Casini, S. Piantelli, A. Ono, E. Bonnet, R. Alba, S. Barlini, B. Borderie, R. Bougault, C. Ciampi *et al.*, Phys. Rev. C **103**, 014605 (2021).

[10] S. Piantelli, G. Casini, A. Ono, G. Poggi, G. Pastore, S. Barlini, A. Boiano, E. Bonnet, B. Borderie, R. Bougault *et al.*, Phys. Rev. C **101**, 034613 (2020).

[11] F. Bocage, J. Colin, M. Louvel, G. Auger, C. Bacri, N. Bellaize, B. Borderie, R. Bougault, R. Brou, P. Buchet *et al.*, Nucl. Phys. A **676**, 391 (2000).

[12] A. B. McIntosh, S. Hudan, J. Black, D. Mercier, C. J. Metelko, R. Yanez, R. T. de Souza, A. Chbihi, M. Famiano, M. O. Frégeau, J. Gauthier, J. Moisan, R. Roy, S. Bianchin, C. Schwarz, and W. Trautmann, Phys. Rev. C **81**, 034603 (2010).

[13] B. Harvey, M. Youngs, A. B. McIntosh, A. Jedele, A. Abbott, J. Gauthier, K. Hagel, A. Hannaman, A. Hood, K. Krieble, Y.-W. Lui, L. A. McIntosh, A. Rodriguez Manso, M. Sorensen, Z. Tobin, R. Wada, A. Zarrella, and S. J. Yennello, Phys. Rev. C **102**, 064625 (2020).

[14] A. Ono, H. Horiuchi, T. Maruyama, and A. Ohnishi, Phys. Rev. Lett. **68**, 2898 (1992).

[15] A. Ono, Phys. Rev. C **59**, 853 (1999).

[16] A. Ono, S. Hudan, A. Chbihi, and J. D. Frankland, Phys. Rev. C **66**, 014603 (2002).

[17] A. Ono, J. Phys.: Conf. Ser. **420**, 012103 (2013).

[18] A. Ono, J. Phys.: Conf. Ser. **569**, 012086 (2014).

[19] H. Morgenstern, W. Bohne, W. Galster, K. Grabisch, and A. Kyanowski, Phys. Rev. Lett. **52**, 1104 (1984).

[20] R. Bougault, G. Poggi, S. Barlini, B. Borderie, G. Casini, A. Chbihi, N. Le Neindre, M. Parlog, G. Pasquali, and S. Piantelli *et al.*, Eur. Phys. J. A **50**, 47 (2014).

[21] S. Valdré *et al.*, Nucl. Instrum. Methods Phys. Res., Sect. A **930**, 27 (2019).

[22] G. Pastore, D. Gruyer, P. Ottanelli, N. L. Neindre, G. Pasquali, R. Alba, S. Barlini, M. Bini, E. Bonnet, B. Borderie *et al.*, Nucl. Instrum. Methods Phys. Res., Sect. A **860**, 42 (2017).

[23] G. Pasquali, G. Pastore, N. Le Neindre, G. Ademard, S. Barlini, M. Bini, E. Bonnet, B. Borderie, R. Bougault, and G. Casini *et al.*, Eur. Phys. J. A **50**, 86 (2014).

[24] S. Carboni, S. Barlini, L. Bardelli, N. L. Neindre, M. Bini, B. Borderie, R. Bougault, G. Casini, P. Edelbruck, A. Olmi *et al.*, Nucl. Instrum. Methods Phys. Res., Sect. A **664**, 251 (2012).

[25] D. Lacroix, A. Van Lauwe, and D. Durand, Phys. Rev. C **69**, 054604 (2004).

[26] R. J. Charity, Phys. Rev. C **82**, 014610 (2010).

[27] S. Piantelli, G. Casini, A. Ono, G. Poggi, G. Pastore, S. Barlini, M. Bini, A. Boiano, E. Bonnet, B. Borderie *et al.*, Phys. Rev. C **103**, 014603 (2021).

[28] C. Frosin *et al.*, arXiv:2303.17390 [nucl-ex] [Phys. Rev. C (to be published)].

[29] C. Ciampi, S. Piantelli, G. Casini, G. Pasquali, J. Quicray, L. Baldesi, S. Barlini, B. Borderie, R. Bougault, A. Camaiani, A. Chbihi, D. Dell'Aquila, M. Cicerchia, J. A. Dueñas, Q. Fable, D. Fabris, J. D. Frankland, C. Frosin, T. Génard, F. Gramegna *et al.* (INDRA-FAZIA Collaboration), Phys. Rev. C **106**, 024603 (2022).

[30] S. Piantelli, A. Olmi, P. R. Maurenzig, A. Ono, M. Bini, G. Casini, G. Pasquali, A. Mangiarotti, G. Poggi, A. A. Stefanini, S. Barlini, A. Camaiani, C. Ciampi, C. Frosin, P. Ottanelli, and S. Valdré, Phys. Rev. C **99**, 064616 (2019).

[31] A. Raduta, B. Borderie, E. Geraci, N. Le Neindre, P. Napolitani, M. Rivet, R. Alba, F. Amorini, G. Cardella, M. Chatterjee, E. De Filippo, D. Guinet, P. Lautesse, E. La Guidara, G. Lanzalone, G. Lanzano, I. Lombardo, O. Lopez, C. Maiolino, A. Pagano *et al.*, Phys. Lett. B **705**, 65 (2011).

[32] B. Borderie, A. Raduta, G. Ademard, M. Rivet, E. De Filippo, E. Geraci, N. Le Neindre, R. Alba, F. Amorini, G. Cardella, M. Chatterjee, D. Guinet, P. Lautesse, E. La Guidara, G. Lanzalone, G. Lanzano, I. Lombardo, O. Lopez, C. Maiolino, A. Pagano *et al.*, Phys. Lett. B **755**, 475 (2016).

[33] F. Amorini, G. Cardella, G. Giuliani, M. Papa, C. Agodi, R. Alba, A. Anzalone, I. Berceanu, S. Cavallaro, M. B. Chatterjee, R. Coniglione, E. De Filippo, A. Di Pietro, E. Geraci, L. Grassi, A. Grzeszczuk, P. Figuera, E. La Guidara, G. Lanzalone, N. Le Neindre *et al.*, Phys. Rev. Lett. **102**, 112701 (2009).

[34] P. Eudes, Z. Basrak, F. Sébille, V. de la Mota, and G. Royer, Phys. Rev. C **90**, 034609 (2014).

[35] R. J. Charity, Phys. Rev. C **58**, 1073 (1998).

[36] V. E. Viola, K. Kwiatkowski, and M. Walker, Phys. Rev. C **31**, 1550 (1985).

[37] K. X. Jing *et al.*, Nucl. Phys. A **645**, 203 (1999).

[38] T. Fan, K. Jing, L. Phair, K. Tso, M. McMahan, K. Hanold, G. Wozniak, and L. Moretto, Nucl. Phys. A **679**, 121 (2000).

[39] D. Hinde, J. Leigh, J. Bokhorst, J. Newton, R. Walsh, and J. Boldeman, Nucl. Phys. A **472**, 318 (1987).

[40] G. Verde, D. A. Brown, P. Danielewicz, C. K. Gelbke, W. G. Lynch, and M. B. Tsang, Phys. Rev. C **65**, 054609 (2002).

[41] G. Verde, P. Danielewicz, W. Lynch, C. Chan, C. Gelbke, L. Kwong, T. Liu, X. Liu, D. Seymour, R. Shomin, W. Tan, M. Tsang, A. Wagner, H. Xu, D. Brown, B. Davin, Y. Larochelle, R. de Souza, R. Yanez, R. Charity *et al.*, Phys. Lett. B **653**, 12 (2007).

[42] D. Drijard, H. Fischer, and T. Nakada, Nucl. Instrum. Methods Phys. Res. **225**, 367 (1984).

[43] Z. Chajęcki and M. Lisa, Phys. Rev. C **78**, 064903 (2008).

[44] G. Verde *et al.*, Eur. Phys. J. A **30**, 81 (2006).

[45] W. P. Tan, W. G. Lynch, T. X. Liu, X. D. Liu, M. B. Tsang, G. Verde, A. Wagner, H. S. Xu, B. Davin, R. T. de Souza, Y. Larochelle, R. Yanez, R. J. Charity, and L. G. Sobotka, Phys. Rev. C **69**, 061304(R) (2004).

[46] B. Borderie, A. Raduta, E. De Filippo, E. Geraci, N. L. Neindre, G. Cardella, G. Lanzalone, I. Lombardo, O. Lopez, C. Maiolino, A. Pagano, M. Papa, S. Pirrone, F. Rizzo, and P. Russotto, Symmetry **13**, 1562 (2021).

[47] D. Dell'Aquila, I. Lombardo, G. Verde, M. Vigilante, L. Acosta, C. Agodi, F. Cappuzzello, D. Carbone, M. Cavallaro, S. Cherubini, A. Cvetinovic, G. D'Agata, L. Francalanza, G. L. Guardo, M. Gulino, I. Indelicato, M. La Cognata, L. Lamia, A. Ordine, R. G. Pizzone *et al.*, Phys. Rev. Lett. **119**, 132501 (2017).

[48] L. Morelli, M. Bruno, M. D'Agostino, G. Baiocco, F. Gulminelli, U. Abbondanno, S. Barlini, M. Bini, G. Casini, M. Cinausero, M. Degerlier, D. Fabris, F. Gramegna, J. Mabiala, T. Marchi, A. Olmi, G. Pasquali, S. Piantelli, and S. Valdré, J. Phys. G: Nucl. Part. Phys. **43**, 045110 (2016).

[49] T. K. Nayak, T. Murakami, W. G. Lynch, K. Swartz, D. J. Fields, C. K. Gelbke, Y. D. Kim, J. Pochodzalla, M. B. Tsang, H. M. Xu, F. Zhu, and K. Kwiatkowski, Phys. Rev. C **45**, 132 (1992).

[50] J. Pochodzalla, C. K. Gelbke, W. G. Lynch, M. Maier, D. Ardouin, H. Delagrange, H. Doubre, C. Grégoire, A. Kyanowski, W. Mittig, A. Péghaire, J. Péter, F. Saint-Laurent, B. Zwieglinski, G. Bizard, F. Lefèbvres, B. Tamain, J. Québert, Y. P. Viyogi, W. A. Friedman *et al.*, Phys. Rev. C **35**, 1695 (1987).

[51] J. Manfredi, R. J. Charity, K. Mercurio, R. Shane, L. G. Sobotka, A. H. Wuosmaa, A. Banu, L. Trache, and R. E. Tribble, Phys. Rev. C **85**, 037603 (2012).

[52] See https://www.nndc.bnl.gov/nudat3/ for ^{13}C.